# Improved Workability of the Nanocomposited $AgSnO_2$ Contact Material and Its Microstructure Control During the Arcing Process

YAPING WANG and HAIYAN LI

There are two major weaknesses for the $AgSnO_2$ contacts used in the low voltage switch devices. One is poor workability, which causes the $AgSnO_2$ materials to hardly deform into the required shape. Another is the increased contact resistance after arcing, which, in turn, causes an unfavorable temperature rise in the switches. In this article, the nanocomposited $AgSnO_2$ materials were developed to overcome the weaknesses. The nanosized $SnO_2$ powders with or without CuO additive were prepared by the chemical precipitation method. The $SnO_2$ powders and Ag powders were high energy milled together to obtain $AgSnO_2$ composite powders, which were then sintered, hot pressed and extruded. It was found that the $SnO_2$ particles mainly distribute in the interior of Ag grains with Ag film on the grain boundary. The hardness of $AgSnO_2$ composites and the wetting angle of Ag melt on $SnO_2$ particles decreased with the addition of a small amount of CuO. By the combining effect of Ag film on grain boundary and the addition of CuO, the elongation and workability of the $AgSnO_2$ materials improved. The experiments of rapid solidification revealed that more $SnO_2$ particles with CuO addition were engulfed in the Ag matrix than those without CuO, which inhibited the redistribution of $SnO_2$ particles on the contact surface during the arcing process. The industrial type test in the 45A contactor suggested that the nanocomposited $AgSnO_2$ materials are suitable to be used as contacts in low voltage switches.

DOI: 10.1007/s11661-016-3859-y


## I. INTRODUCTION

THE $AgSnO_2$ contacts exhibit good welding resistance and remarkable arc erosion resistance compared with toxic AgCdO.[1–5] Over the last 30 years, there have been considerable investigations on the $AgSnO_2$ contacts replacing the AgCdO contacts used in low voltage switching devices.[6–8] It is found that the workability of $AgSnO_2$ is poor so that it is difficult, for instance, to produce rivets with high head-to-shank ratios or to roll strip materials with large deformation.[9] Another disadvantage is the high temperature rise and high contact resistance of $AgSnO_2$ contacts in service because of the formation of $SnO_2$-rich layer on the contact surface after repeated arcing.[10–12] These two weaknesses limit the commercial manufacture and application of the $AgSnO_2$ contacts.

The low ductility of $AgSnO_2$ materials attributes to the higher hardness of $SnO_2$ particles than the CdO particles in AgCdO contacts. Another reason for the inadequate workability is that the $SnO_2$ particles tend to distribute at the Ag grain boundaries by conventional powder metallurgy or internal oxidation techniques.[13,14] The hard $SnO_2$ particles cause stress concentrations at the Ag grain boundaries and lead to crack near them. The elongation (EL), therefore, was endangered by the formation of voids or cracks at the grain boundaries.

For the AgMeO contacts, the switching behavior depends greatly on microstructure, especially on the size and dispersion of the MeO particles.[15,16] When the particle size decreases, the anti-welding and anti-erosion properties increase. Nevertheless, the size reduction of $SnO_2$ particles, for achieving better properties, will generally reduce ductility and workability of $AgSnO_2$ materials further.

In order to solve the problem of poor workability and simultaneously achieve better properties of $AgSnO_2$ materials, we propose a strategy—refining the $SnO_2$ particles to nanoscale and spreading them into the Ag grain interior, rather than making them coarsen and concentrate at the grain boundaries. This method could encourage entrapment by the $SnO_2$ particles in the interior of the grain, which may be helpful to maintain deformation strengthening and uniform EL and, therefore, increased ductility.

To prevent the formation of $SnO_2$-rich layer on the arcing surface, it is necessary to control the redistribution behavior of the $SnO_2$ particles during repeated arcing process, which causes instantaneous melting of a

YAPING WANG, Professor, is with the MOE Key Laboratory for Non-equilibrium Synthesis and Modulation of Condensed Matter, School of Science, Xi an Jiaotong University, Xi an 710049, P.R. China, and also with the State Key Laboratory for Mechanical Behavior of Materials, Xi an 710049, P.R. China. Contact e-mail: ypwang@mail.xjtu.edu.cn HAIYAN LI, Postdoctoral Candidate, is with the MOE Key Laboratory for Non-equilibrium Synthesis and Modulation of Condensed Matter, School of Science, Xi an Jiaotong University.

Manuscript submitted January 5, 2016.
Article published online November 23, 2016

thin surface layer of contact and then rapid solidification due to rapid heat extraction to the unmelted contact substrate.[17] The redistribution of $SnO_2$ particles in $AgSnO_2$ materials is assumed to occur during the rapid melting and subsequent rapid solidification. However, it is difficult to *in-situ* study the microstructure modification during the arcing process because of the extremely short arcing duration. The rapid solidification is considered to be a natural result of arcing so that the redistribution of $SnO_2$ particles in $AgSnO_2$ materials is assumed to occur during rapid solidification. The traditional rapid solidification technology under different environments, therefore, is used to create similar arcing conditions to study the redistribution behavior of $SnO_2$ particles. The effect of the wetting ability of silver melt on the $SnO_2$ particles is emphasized.

In this article, $AgSnO_2$ nanocomposited powders with the addition of CuO were prepared by high energy milling, which was performed to disperse the nano-sized oxide particles into the grain interior by high milling energy. The simultaneous rapid solidification experiments were conducted to study the redistribution behavior of $SnO_2$ particles. After the cold press, sintering and hot press of $AgSnO_2$ nanocomposited powders, the ductility and microhardness of the $AgSnO_2$ nanocomposited materials were investigated. The $AgSnO_2$ nanocomposite materials with optimized composition were industrial manufactured by sintering, hot extrusion and cold drawing. The type test was conducted to examine the comprehensive properties of the contacts.

## II. EXPERIMENTAL

### A. *Powder Preparation*

The pure $SnO_2$ powders and the $SnO_2$ powders with CuO additive were prepared by the precipitation method. A calculated amount of nitrate copper was added to an aqueous solution of $SnCl_2$, and then ammonia was added to the solution. The solution was stirred at 363 K (90 °C) by the magnetic stirring apparatus to promote hydrolysis followed by filtering. After washing with deionized water and absolute alcohol, the precipitate was dried at atmosphere overnight followed by calcining in a muffle furnace at 873 K (600 °C) for 2 hours. The obtained $SnO_2$ powders and the $SnO_2$ powders with CuO additives were analyzed by a 7000S X-ray diffractometer using Cu$K_\alpha$ radiation ($\lambda$ = 1.54060 A) and ESCALAB250 X-ray photoelectron spectroscopy (XPS).

The wetting angles of $SnO_2$ particles containing different CuO content additives by molten silver were measured by the sessile drop technique. Cross sections of the interface between solidified silver and oxides were investigated by a JEOL JSM-6301F scanning electron microscope (SEM). The composition distribution in the interface area was determined by an electron-probe microanalyzer (EPMA).

### B. *Preparation of the Nanocomposited $AgSnO_2$ Materials and Their Mechanical Properties*

The 88 wt pct pure silver powder with size less than 74 $\mu$m and the 12 wt pct prepared tin oxide powders were milled in Simloyer-20L high energy miller under sealing atmosphere with a constant ball-to-powder weight ratio of 10:1. The milling time was set as 1 hour. The ball-milled powders were annealed at 673 K (400 °C) for 2 hours to release milling stress. The $AgSnO_2$ powders were compacted under a pressure of 200 MPa, sintered at 1173 K (900 °C) for 1 hour, and further hot pressed under a pressure of 20 MPa. The microstructure of the milled powders and hot-pressed compacts were observed by the SEM and TEM-200CX transmission electron microscope (TEM).

Microhardness measurements of the sintered and hot-pressed compacts were performed using a macro-Vickers tester. The microhardnesses were measured under 10-gf load for 10 seconds on the oxide- and silver-rich areas and 1 kgf for 5 seconds on the large silver-rich area. Ten tests of microhardness for each compact were used, and the mean value was taken as the accepted value. The formability of compacts was determined by measuring the percent EL of the hot-pressed compacts during the cold-rolling experiment. The compact with a composition of 88 wt pct Ag, 11.4 wt pct $SnO_2$, and 0.6 wt pct CuO, which exhibited good ductility in the cold-rolling test, was industrial manufactured by hot extrusion and cold drawing.

### C. *Simulation of Arcing Process by Rapid Solidification*

Some rapid solidification experiments were processed by the melt-spinning method. The $AgSnO_2$ samples were melted in a quartz tube and quenched onto a copper wheel rotating at a tangential speed of 4 m/s. HF induction melting in an $Al_2O_3$ crucible was preformed and the melts were *in-situ* solidified spontaneously by placing the crucible into water. The rapid solidification experiments were also carried out under the static

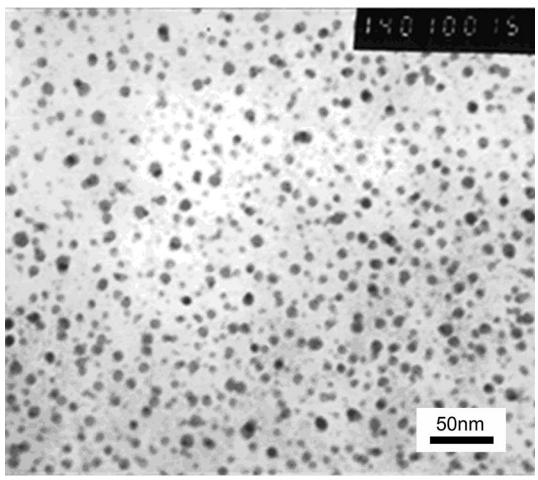


Fig. 1—Typical morphology of $SnO_2$ powders.

magnetic field of 1 T. The magnetic field was kept constant until the melting and solidification were finished.

### D. *Type Test*

The type test for the CJX4-63 contactor was made to examine the feasibility of this kind of $AgSnO_2$ nanocomposited material in industry. The rivet samples were made from the as-drawn $AgSnO_2$ wires.

## III. RESULTS AND DISCUSSION

### A. *Characterization of $SnO_2$ Powders*

Figure 1 is the typical morphology of $SnO_2$ powders. It can be seen that the $SnO_2$ powders display nearly sphere. The mean particle size is about 10 nm.

The XRD patterns of pure $SnO_2$ and CuO-doped $SnO_2$ nanoparticles are shown in Figure 2. It can be seen that typical peaks of $SnO_2$ crystals detected in the XRD patterns agree well with those of the JCPDS date (Card No. 41-1445) and could be fitted with the tetragonal rutile structure. The spectra of CuO-doped $SnO_2$ show a new diffraction peak corresponding to the (002) plane of the monoclinic CuO (JCPDS Card No. 45-0937) along with $SnO_2$ peaks, which illustrates the formation of CuO.[18] The XRD peaks of the CuO-doped $SnO_2$ nanoparticles are more intense than those of the pure $SnO_2$ nanoparticles, indicating the higher crystalline nature and increased particle size of the $SnO_2$ nanoparticles with CuO addition. This finding means that CuO promoted the crystal formation and growth of $SnO_2$ particles during calcining.

As seen in Figure 3, the Cu element detected on the surface of the sample by means of XPS analysis is confirmed to be $Cu^{2+}$, corresponding to CuO. The

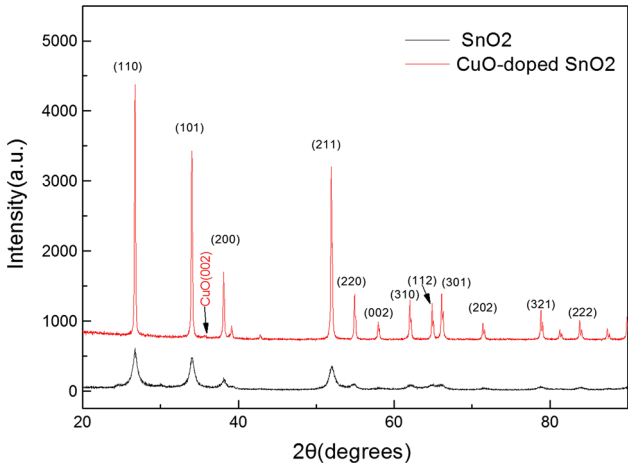


Fig. 2—XRD patterns of pure $SnO_2$ and CuO-doped $SnO_2$ nanoparticles.

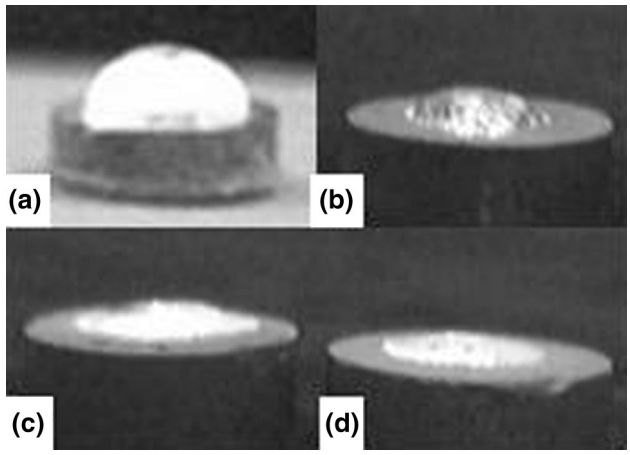


Fig. 4—Wetting angles of Ag melts on $SnO_2$ bulks with different CuO contents: (*a*) $SnO_2$, (*b*) $SnO_2$ + 3 pct CuO, (*c*) $SnO_2$ + 5 pct CuO, and (*d*) $SnO_2$ + 7 pct CuO.

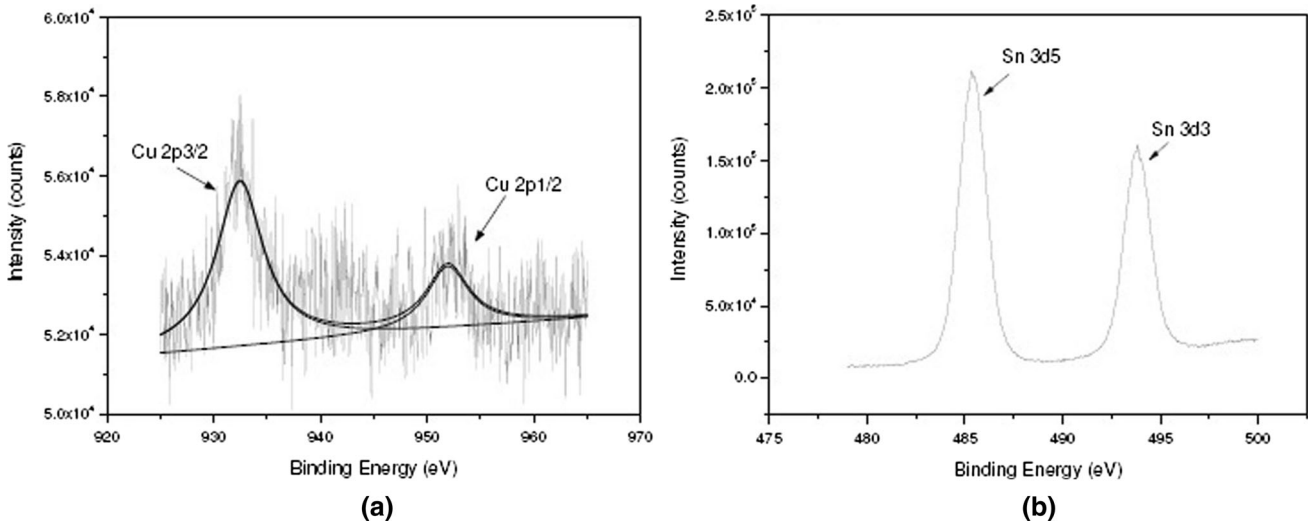


Fig. 3—XPS spectra of CuO-doped $SnO_2$ powder: (*a*) Cu 2p scan and (*b*) Sn 3d scan.

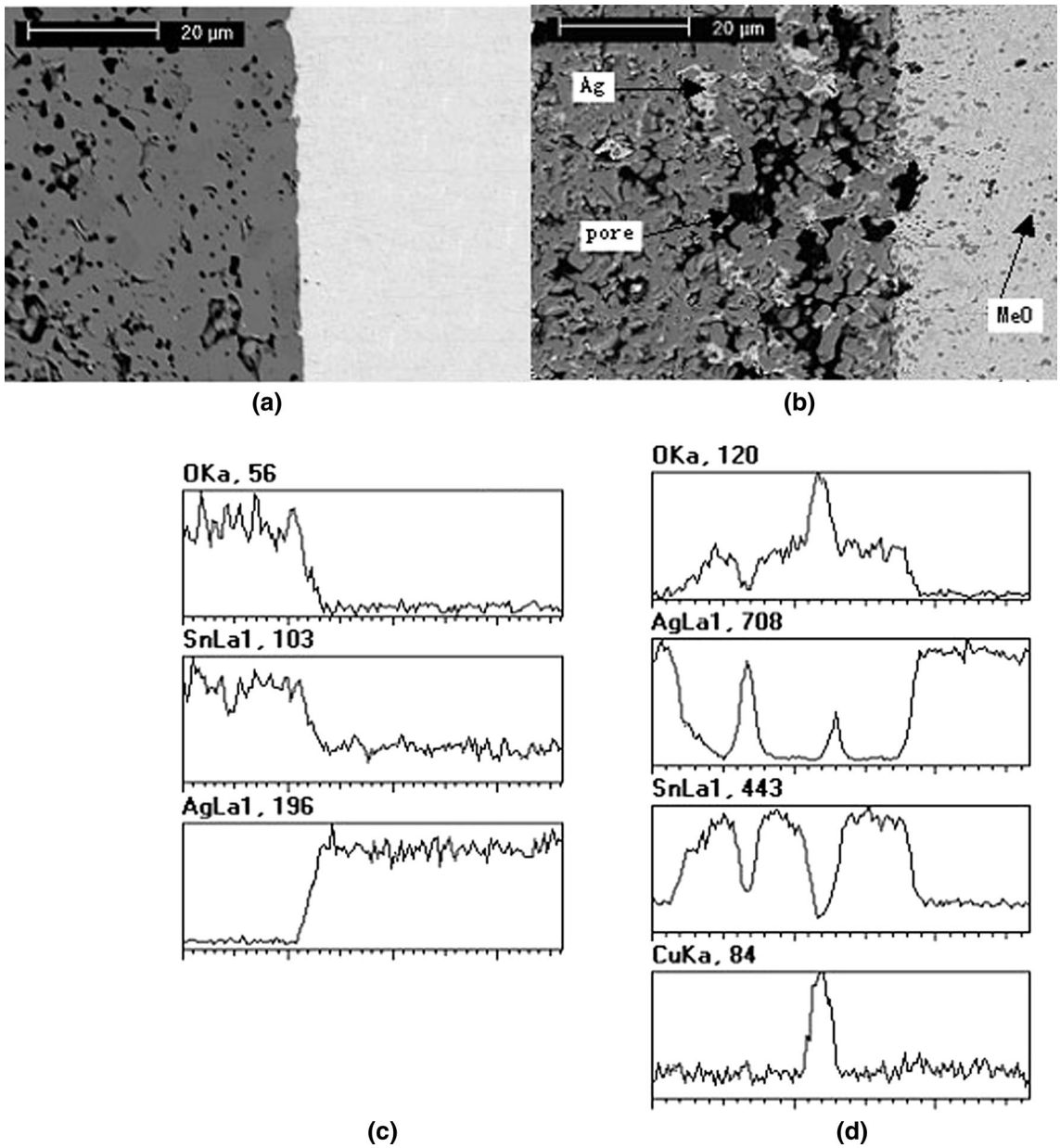


Fig. 5—Cross-sectional microstructure of interfaces for solidified silver and $SnO_2$ substrates: (*a*) Ag-$SnO_2$, (*b*) Ag-$SnO_2$CuO, (*c*) EPMA line analyses corresponding to (a), and (*d*) EPMA line analyses corresponding to (b).

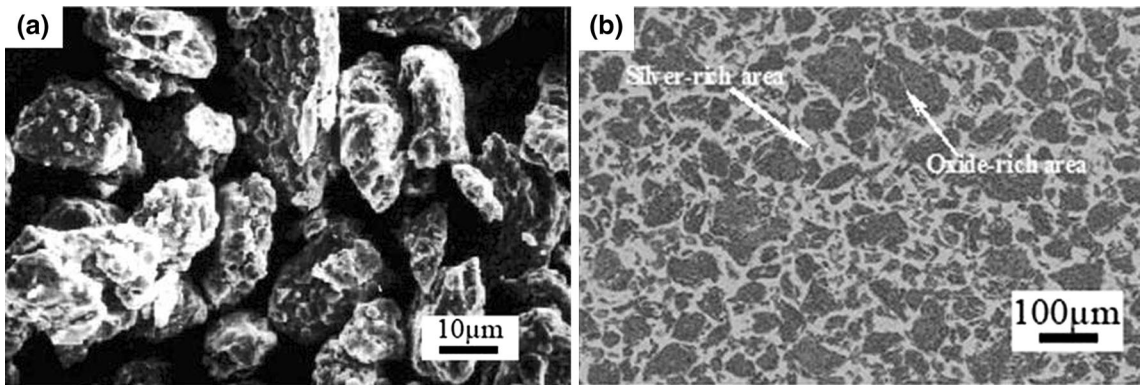


Fig. 6—Microstructure of Ag-$SnO_2$ powder and compact: (*a*) high energy milled powder and (*b*) hot-pressed compact.

valence state of the Sn ion experiences no change with the addition of CuO. It could be inferred by the XPS results that CuO did not solve in the $SnO_2$ phase but existed solely on the surface of the $SnO_2$ particles, which should result from the first precipitation of $Sn(OH)_4$ followed by that of $Cu(OH)_2$.

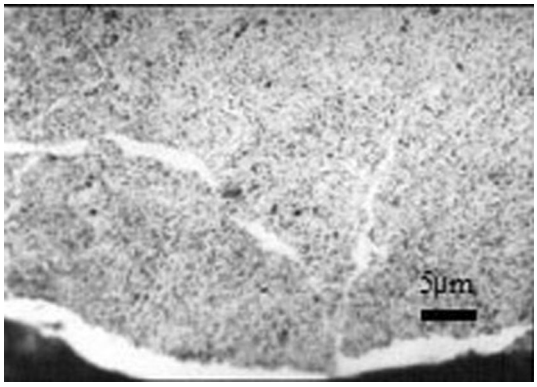


Fig. 7—Microstructure of high energy milled $AgSnO_2$ powders after annealing at 673 K (400 °C).

### B. *Effect of CuO Addition on the Wettability and Interface Characteristics between $SnO_2$ and Molten Silver*

The wettability of $SnO_2$ bulks by Ag droplets is shown in Figure 4. The wettability of the Ag droplet and $SnO_2$ without CuO doping is poor, with a wetting angle of about 90 deg, as shown in Figure 4(a). The wetting angle reduces remarkably with the addition of CuO. Figures 4(b) and (c) show that the wetting angles of Ag droplet on $SnO_2$ decrease to 53 deg with 3 pct CuO and 38 deg with 5 pct CuO, respectively. The wetting angle of Ag droplet on $SnO_2$ with 7 pct CuO addition in Figure 4(d) is only 29 deg, indicating that the wettability of CuO-doped $SnO_2$ by liquid silver is dramatically improved.[19]

It is observed in Figure 5(a) that the boundary between pure $SnO_2$ and the Ag droplet is clear and smooth, but there is an interfacial transition layer between CuO-doped $SnO_2$ and Ag, as shown in Figure 5(b). Figure 5(a) shows that little silver phase (light zone) appears in the side of the pure $SnO_2$ near the interface. However, for the $SnO_2$ bulk with CuO addition, the molten silver deeply infiltrates into the solid phase and, meanwhile, large amounts of MeO containing $SnO_2$ and CuO particles (arrow) diffuse into the liquid silver (Figure 5(b)). Figure 5(c) shows the EPMA line between pure $SnO_2$ and Ag corresponding to

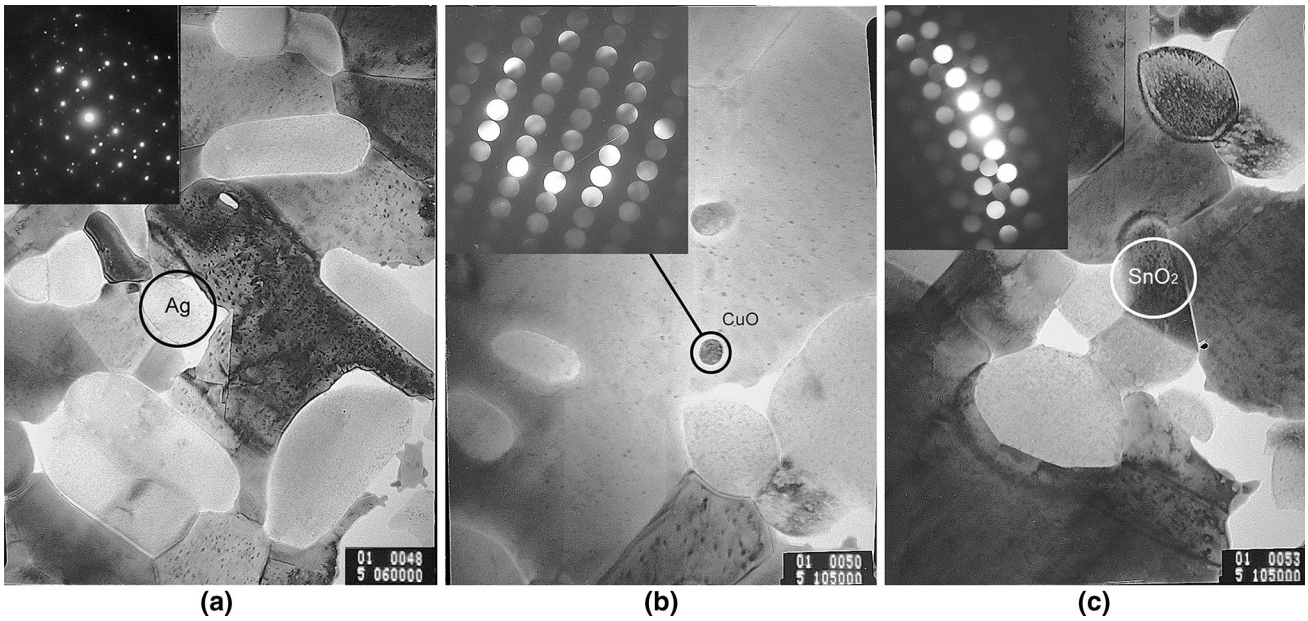


Fig. 8—TEM bright field images of hot-pressed $AgSnO_2CuO$ compacts of the selected area (*a*) Ag, (*b*) CuO, and (*c*) $SnO_2$.

**Table I. Microhardness and EL of the $AgSnO_2$ Compacts**

| | Microhardness (HV) | | | |
|---|---|---|---|---|
| Sample | Oxide-Rich Area (10 g Load) | Silver-Rich Area (10 g Load) | Silver-Rich Area (1 kg Load) | EL (Pct) |
| $AgSnO_212$ | 157.6 | 101.7 | 108.2 | 12.6 |
| $AgSnO_211.4CuO0.6$ | 131.3 | 88.8 | 94.1 | 43.6 |
| $AgSnO_211.16CuO0.84$ | 101.8 | 82.3 | 80.5 | 55 |

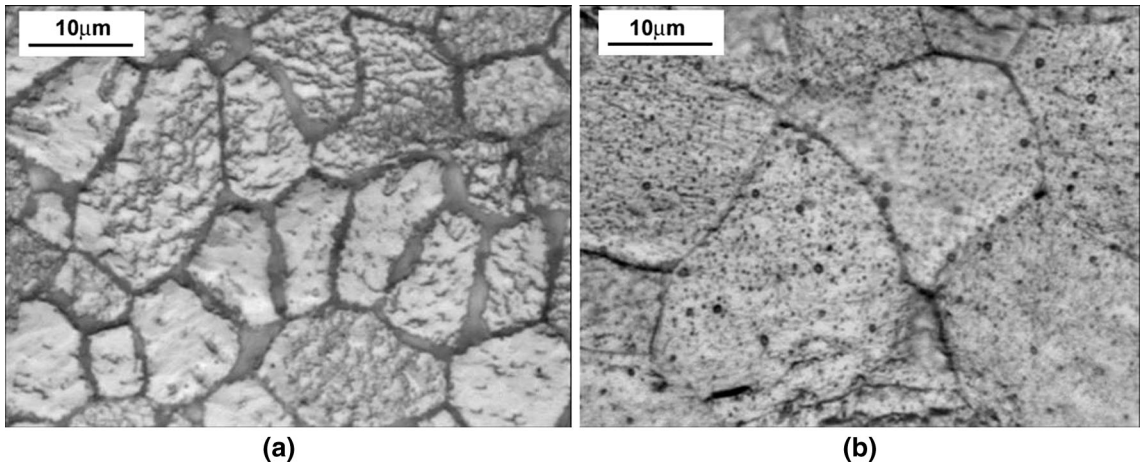


Fig. 9—Ribbon microstructure: (*a*) $AgSnO_2$ and (*b*) $AgSnO_2CuO$.

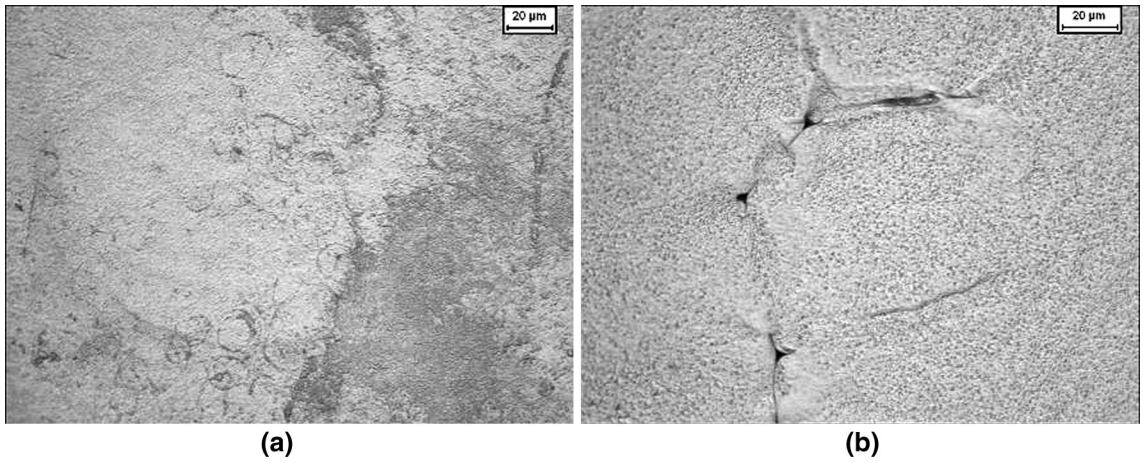


Fig. 10—Solidification microstructures under high magnetic field (1 T): (*a*) $AgSnO_2$ and (*b*) $AgSnO_2CuO$.

**Table II. Type Test of $AgSnO_2CuO$ Materials**

| Conditions | AC-3 | | | | |
|---|---|---|---|---|---|
| Rated value | 380 V, 60 A | | | | |
| Items | make operations | make-break ability | | conventional working capability | |
| Parameters | make | make | break | make | break |
| Voltage | 400 V | 400 V | 400 V | 400 V | 400 V |
| Current | 602 A | 483 A | 483 A | 126 A | 126 A |
| Cos$\varphi$ | 0.47 | 0.49 | 0.49 | 0.44 | 0.44 |
| Number of operations | 50 | 50 | | 6000 | |
| Temperature rise | 49.4 K (49.4 °C) | | | | |
| Contact resistance | Phase A | Phase B | | Phase C | |
| | 2.9 mΩ | 4.1 mΩ | | 5.1 mΩ | |

Figure 5(a). There is an obvious boundary line between the left $SnO_2$ zone and the right Ag zone. On the other hand, the boundary line disappears in Figure 5(d), corresponding to the results of Figure 5(b), indicating the increased interdiffusion between silver and $SnO_2$ with CuO addition. The change of the infiltration ability comes from the enhanced wettability between the Ag melt and $SnO_2$ particles by the CuO additive.

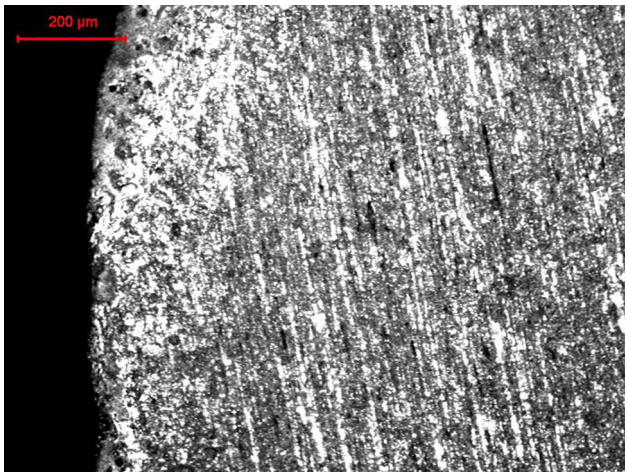


Fig. 11—Microstructure of $AgSnO_2$ nanocomposited materials after 15,000 times making and breaking operations.

### C. *Microstructures of $AgSnO_2$ Materials with and Without CuO Additive*

Figure 6(a) shows that the high energy milled Ag-$SnO_2$ powders display irregular shape with an average size of 20 $\mu$m. Figure 6(b) illustrates the microstructure of hot-pressed $AgSnO_2$ materials. The light gray area is the Ag-rich region, and the black area is the mixing region of Ag and oxides. The oxide-rich islands are separated by the network of the silver-rich region.

The Ag-rich regions in the $AgSnO_2$ compacts are beneficial to the plastics of the materials, because they could allow avoidance of the initiation of crack in the grain boundary, which is the weakness of the traditional $AgSnO_2$ materials. In order to investigate the formation reason of the Ag-rich region in the hot-pressed compacts, the milled $AgSnO_2$ powders were annealed at 673 K (400 °C) for 1 hour, and their microstructure is shown in Figure 7. It is also found that Ag-rich film formed around the grain boundary and the particle edge, suggesting that the ex-diffusion of the silver occurs during the sintering of the $AgSnO_2$ compacts.[20] During the process of high energy milling, the hard and brittle $SnO_2$ pinned into the soft silver matrix and induced severe stress. When the powders or the cold-pressed compacts were heated, the stress could induce the ex-diffusion of silver from the grain interior to the boundary or the powder edge. The final distribution of Ag-rich region around grain boundary could improve the formability of the $AgSnO_2$ materials.

Figure 8 shows the high-resolution images of $AgSnO_2$ contacts. From the diffraction spots, the components of Ag, CuO, and $SnO_2$ were detected separately, which confirms the existence of CuO addition as CuO particles, as obtained in XPS results.

### D. *Mechanical Properties of $AgSnO_2$ Materials*

The microhardness on the different phases in the $AgSnO_2$ materials and the EL during roll experiments are listed in Table I. It can be seen that the microhardness of the oxide-rich area is much higher than that of the silver-rich area, corresponding to Figure 6(b). The hardness of samples decreases significantly with the increase of CuO content. Elongation of $AgSnO_2$ samples with the CuO addition could increase more than 3 times than that without CuO, suggesting the significant effect of CuO on the plastic deformation ability.

### E. *Microstructure of $AgSnO_2$ Composites During Rapid Solidification*

Figure 9 shows the melt-spinning microstructure of $AgSnO_2$ samples with and without CuO. Figure 9(a) shows that the $SnO_2$ particles in $AgSnO_2$ are more confined at grain boundaries than engulfed in Ag matrix.

However, for the $AgSnO_2$CuO ribbon samples, some $SnO_2$ particles are found to distribute uniformly in the melt-spinning microstructure, as shown in Figure 9(b), indicating that the addition of CuO promotes the engulfing of the $SnO_2$ particles in the Ag melt under the rapid solidification conditions.[17]

The improvement of the engulfment of the $SnO_2$ particles in the Ag melt during rapid solidification is a benefit of retarding the formation of $SnO_2$ layer on the contact surface after repeated arcing processes, which could be qualitatively explained by Stafanescu's kinetic model for particle engulfment.[21] The addition of CuO increases the size of MeO particles (as obtained in Figure 2 by X-ray analysis) and the wettability between the Ag melts and MeO particles (as shown in Figures 4 and 5) so that the critical solidification velocity for particle engulfing decreases, which makes the $SnO_2$ particles more easily engulfed.

Figure 10 shows the influence of magnetic field on the redistribution behaviors of $SnO_2$ in Ag melts. Under the high magnetic field, the engulfing ability improves for both the pure $SnO_2$ particles and those with CuO addition in molten silver so that more $SnO_2$ particles can be found in the quenched $AgSnO_2$ bulks, as in Figure 10(a) for pure $SnO_2$ and Figure 10(b) with CuO additive. However, there are still more $SnO_2$ particles with CuO addition engulfed in the Ag matrix, confirming further the increased engulfing effect of CuO for $SnO_2$ particles in Ag melts.

### F. *Results of Type Test*

Table II summarizes the type test results in the CJX4-63 contactor by using the $AgSnO_2$ contacts with 0.6 wt pct CuO addition. The contactor finishes 15,000 times making and breaking experiments. The microstructure of $AgSnO_2$ materials after 15,000 times breaking is observed with no obvious $SnO_2$ aggregation on the contact surface, as in Figure 11. The temperature rise and contact resistance remain below 49.4 K (49.4 °C) and 5.1 mΩ after 15,000 arcing operations, indicating that the properties of the nanocomposited

$AgSnO_2$ materials meet the needs of commercial switches.

## IV. CONCLUSIONS

The nanocomposited $AgSnO_2$ materials are prepared by high energy milling and subsequent sintering, hot pressing, and extrusion processes, in which the $SnO_2$ particles mainly distribute in the interior of Ag grains with Ag film on the grain boundary. The EL and workability of the $AgSnO_2$ materials improved obviously for the effect of Ag film and the addition of CuO. During the rapid solidification process, more $SnO_2$ particles with CuO addition were engulfed in the Ag matrix, which is beneficial to inhibiting the redistribution of $SnO_2$ particles on the contact surface after the repeated arcing process. The type test results indicate that the nanocomposited $AgSnO_2$ materials are suitable for use in the low voltage switching devices.

## ACKNOWLEDGMENTS

The authors acknowledge Q.B. Ye, J.Z. Wang, J.B. Wang, and H.Y. Liu for their assistance in the sample preparation and analysis. Thanks are also given for the financial support of the National Science Foundation of China (Grant Nos. 51171146 and 51607132) and the Program for Key Science and Technology Innovative Research Team of Shaanxi Province (Grant No. 2013KCT-05).

## REFERENCES

1. P.C. Wingert and C.H. Leung: *IEEE Trans. Comp. Hybrids. Manuf. Technol.*, 1987, vol. 10, pp. 56–62.
2. M. Huck, A. Kraus, R. Michal, and K.E. Saeger: *IEEE*, 1990, pp. 133–38.
3. D. Jeannot, J. Pinard, P. Ramoni, and E.M. Jost: *IEEE*, 1993, pp. 51–59.
4. D. Jeannot, J. Pinard, P. Ramoni, and E.M. Jost: *IEEE Trans. A*, 1994, vol. 17, pp. 17–23.
5. X.M. Liu, S.L. Wu, P.K. Chu, C.Y. Chung, J. Zheng, and S.L. Li: *Mater. Chem. Phys.*, 2006, vol. 98, pp. 477–80.
6. W. Boehm, N. Behrens, and M. Clasing: *Metall.*, 1981, vol. 35, pp. 539–43.
7. J. Feng, J.C. Chen, B. Xiao, and C.T. Zhou: *Phys. B*, 2009, vol. 404, pp. 2461–67.
8. M. Zhang, X.H. Wang, X.H. Yang, J.T. Zou, and S.H. Liang: *Trans. Nonferrous Met. Soc. China*, 2016, vol. 26, pp. 783–90.
9. V. Behrens, T. Honig, A. Kraus, R. Michal, K.E. Saeger, R. Schmidberger, and T. Staneff: *IEEE Trans. CPMT Part A*, 1994, vol. 17, pp. 24 31.
10. N. Lorrain, L. Chaffron, C. Carry, P. Delcroix, and G. Le Caër: *Mater. Sci. Eng. A*, 2004, vol. 367, pp. 1–8.
11. X.M. Liu, S.L. Wu, P.K. Chu, J. Zheng, and S.L. Li: *Mater. Sci. Eng. A*, 2006, vol. 426, pp. 274–77.
12. T. Mützel, P. Braumann, and R. Niederreuther: *IEEE*, 2009, pp. 200–05.
13. P. Verma, O.P. Pandey, and A. Verma: *J. Mater. Sci. Technol.*, 2004, vol. 20, pp. 49–52.
14. Z. Ji, S.L. Li, F.Q. Dou, and T.H. Li: *Rare Met.*, 2009, vol. 28, pp. 19–23.
15. V. Ćosović, A. Ćosović, N. Talijan, D. Živković, and D. Minić: *J. Alloy Compd.*, 2013, vol. 567, pp. 33–39.
16. C.P. Wu, D.Q. Yi, J. Li, L.R. Xiao, B. Wang, and F. Zheng: *J. Alloy Compd.*, 2008, vol. 457, pp. 565–70.
17. Q.B. Ye and Y.P. Wang: *Mater. Sci. Eng. A*, 2007, vol. 449, pp. 1045–48.
18. N. Kumari, A. Ghosh, and A. Bhattacharjee: *Mater. Sci. Semicon. Proc.*, 2014, vol. 19, pp. 114–23.
19. M. Jung, J. Krausmann, M. Bender, J. Bachmann, and J. Rödel: *J. Mater. Sci.*, 2015, vol. 50, pp. 4962–69.
20. G.C. Kuczynski: *AIME Trans.*, 1949, vol. 185, pp. 169–78.
21. D.M. Stefanescu and B.K. Dhindaw: *ASM Int.*, 1988, p. 142.